

Comments on Bona-Massó type slicing conditions in long-term black hole evolutions

David Garfinkle

Department of Physics, Oakland University, Rochester, MI 48309, USA

Carsten Gundlach and David Hilditch

School of Mathematics, University of Southampton, Southampton, SO17 1BJ, UK

We review in generality why time-independent endstates can be reached in black hole and collapse simulations, with and without excision. We characterise the Killing states of the Bona-Massó slicing condition with time derivative along the normals to the slice (“BMn”) as solutions of a mixed elliptic/hyperbolic differential equation on the slice. We show numerically that these steady states can be reached as end states from typical initial data with excision but can be reached with the puncture method only if the puncture is not numerically well resolved. During the evolution, BMn slicings often form gauge shocks. It may be that these are not seen in current 3D simulations only through lack of resolution, although we expect that they can be avoided with some care. Finally we point out that excision with BMn as currently implemented is ill-posed and therefore not expected to converge; this can be cured. In technical appendixes, we derive the equations of pure gauge systems on a fixed spacetime, and bring the BSSN/NOR equations into 3-dimensional tensor form suitable for multiple coordinate patches or spherical polar coordinates.

Contents

I. Introduction	1	B. Wormhole initial data for the Einstein equations	12
II. Numerical evolution of black hole spacetimes	2	C. Reduction of the NOR formulations to spherical symmetry	12
A. Eternal and collapse black holes	2	D. Spherical Einstein-scalar code	12
B. Singularity-avoiding slicings	2	References	13
C. Excision	3		
III. Killing coordinates	3		
A. General case	3	I. INTRODUCTION	
B. Schwarzschild spacetime in spherical symmetry	4		
IV. Evolved slicing conditions	4		
V. Compatibility of Killing coordinates with BMn slicing	5		
A. General	5		
B. Schwarzschild spacetime in spherical symmetry	5		
VI. Vacuum black hole evolutions	6		
A. Method	6		
B. With excision boundary	6		
C. With isometry boundary condition	6		
D. Gauge shocks	7		
VII. Scalar field collapse evolutions	7		
VIII. Conclusions	9		
Acknowledgments	10		
A. Pure gauge evolutions	10		
1. General equations	10		
2. Initial data	11		
3. Characteristic analysis	11		

In 2005, parallel breakthroughs in the long-term stable simulation of binary black holes were made using two rather different approaches: Pretorius [1] used modified harmonic slicing, black holes created in collapse, and singularity excision, while the Brownsville [2] and Goddard [3] groups used eternal black holes, and singularity-avoiding (1+log) slicing. Nevertheless, a key ingredient in both these successes is their gauge choice.

Generalising and extending recent work by Hannam *et al.* [4], we further investigate the application to black hole and collapse spacetimes of the Bona-Massó slicing condition with time derivative along the slice normals (“BMn”). This family includes both the “1+log” slicing used in [2, 3] and the harmonic slicing, a variant of which is used in [1].

A desirable property for a gauge choice is that the metric becomes time-independent to the extent that the spacetime becomes stationary [5]. In Sec. II we explain carefully why this is possible both when the black holes are excised and when a singularity-avoiding slicing is used. We characterise Killing coordinates geometrically in Sec. III. To fix notation, we review various lapse conditions of Bona-Massó type in Sec. IV. In Sec. V we classify Killing slicings compatible with BMn slicing, and in particular the spherical Killing slicings of Schwarzschild

spacetime. In Sec. VI we investigate numerically if any such Killing states are in fact attractors in evolutions of the Schwarzschild spacetime. We consider both slices with wormhole topology and slices which end at an excision boundary inside the black hole. In Sec. VII, we present spherically symmetric simulations of scalar field collapse as a toy model for black holes formed in collapse. From our mathematical and numerical observations in these sections, we suggest improvements to current methods for binary black hole evolutions in Sec. VIII.

II. NUMERICAL EVOLUTION OF BLACK HOLE SPACETIMES

A. Eternal and collapse black holes

Black holes in the real world have formed in collapse, but eternal black holes are often used in numerical relativity because they differ from collapse black holes only in the interior, and this cannot affect physics outside. Here we concentrate on non-rotating, uncharged black holes, which are described by the Kruskal extension of the Schwarzschild spacetime. A bifurcate Killing horizon divides this spacetime into past (P), future (F), “left” (L) and “right” (R) regions. The future and past timelike (i^+ and i^-) and null (\mathcal{I}^+ and \mathcal{I}^-) infinities and the space-like infinity i^0 all exist in left (L) and right (R) copies. Slices extending from i_L^0 to i_R^0 have wormhole geometry, see Fig. 1. Binary (or multiple) black hole initial data can be represented by a wormhole leading to a separate copy of i_L^0 for each black hole. In the “puncture” method [6], each i_L^0 is then represented in coordinates by a point where the conformal factor diverges.

By contrast, black holes formed from regular data through collapse have trivial spatial topology, similar to the Schwarzschild spacetime but with part of R and F, and all of P and L, covered up by the collapsing star [7] – see Fig. 4.

B. Singularity-avoiding slicings

Both in collapse and in eternal black holes one can use slicings which avoid the singularity. Any timelike worldline inside a black hole has finite length, while any timelike worldline with limited total acceleration outside the black hole has infinite length. The lapse measures the rate of proper time per coordinate time for an observer normal to the time slices, and so one might think that the lapse must go to zero everywhere inside the black hole in order to avoid the singularity, and that because the slices keep advancing outside the black hole, their intrinsic geometry must deform without limit as time goes on, until large gradients can no longer be resolved. Such “slice stretching” was indeed encountered in early black hole simulations, and motivated the development of black hole excision [8].

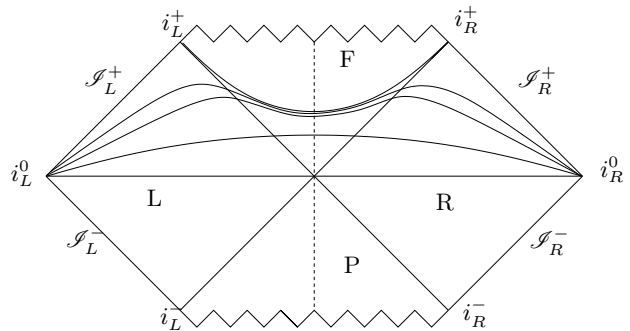


FIG. 1: Spacetime diagram of the Schwarzschild spacetime, with the angular coordinates suppressed. The horizontal line from i_L^0 to i_R^0 is the time-symmetric wormhole slice typically used as initial data in puncture evolutions of a Schwarzschild black holes. The curved lines schematically represent the slicing generated from these initial data by BMn lapse with $\alpha = 1$ initially. They approach the slice $R = R_0$, which links i_L^+ to i_R^+ . The vertical dashed line represents the symmetry boundary which can replace the left-right reflection symmetry of this slicing. As the slices approach $R = R_0$, the approximately cylindrical wormhole grows longer linearly with time.

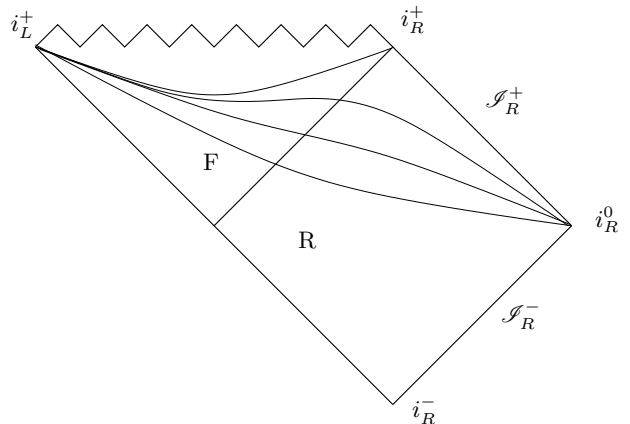


FIG. 2: The same spacetime diagram, schematically showing the unique regular spherical Killing slicing that is compatible with BMn slicing (for a given $\mu_L(\alpha)$). All slices are isometric to one another, and connect i_L^+ with i_R^+ . They again asymptote to the slice $R = R_0$.

Only later it was realised clearly that singularity-avoiding slicings need not lead to slice stretching [9]. If the lapse is chosen such that the slice is Lie-dragged along the Killing vector field everywhere, its intrinsic geometry becomes time-independent. This is true also inside the black hole where the Killing vector field that generates time translations at infinity becomes spacelike (and so the spacetime is not technically stationary), as long as this Killing vector field is nowhere parallel to the slicing. Once the geometry of the slice has become time-independent, a suitable shift condition then makes the spatial metric coefficients explicitly time-independent. With this lapse and shift $\partial/\partial t$ becomes the

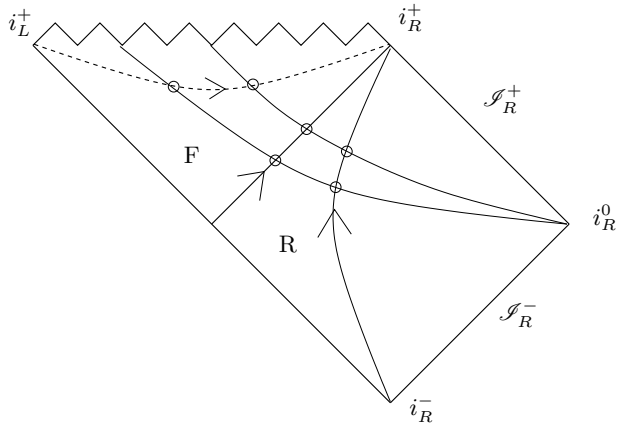


FIG. 3: The same spacetime diagram, schematically showing a Killing slicing that ends at the future singularity, such as Kerr-Schild slices. The lines with arrows are trajectories of the Killing vector (lines of constant R) and the beads on them represent surfaces of constant coordinate r if the Killing shift is used. In particular, the dashed line could serve as a Killing excision boundary.

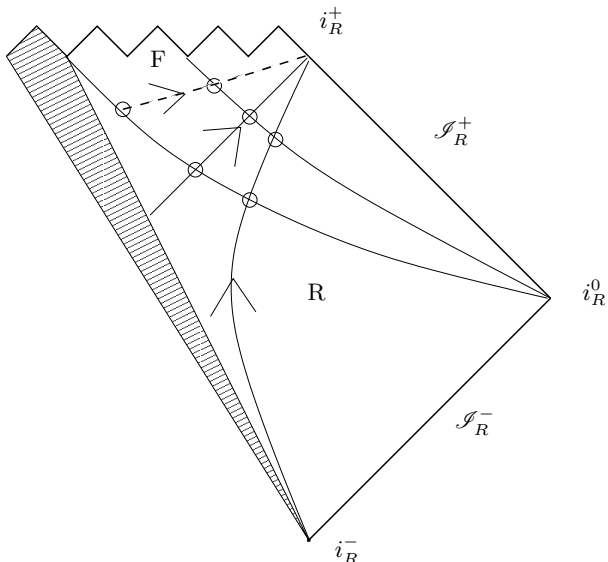


FIG. 4: Schematic spacetime diagram of the collapse of a spherical star. Outside the collapsing star (shaded) the spacetime is Schwarzschild, comprising parts of regions R and F. A Killing slicing with excision as in Fig. 3 is shown. A Killing endstate cannot be reached without excision.

Killing vector (spacelike inside a black hole). Coordinate conditions which generate Killing coordinates asymptotically starting from generic initial coordinates were called “symmetry-seeking” in [5].

Even more recently it was realised that the lapse need not collapse either [4]. Note that

$$\left(\frac{\partial}{\partial t}\right)^a \equiv \alpha n^a + \beta^i \left(\frac{\partial}{\partial x^i}\right)^a \quad (1)$$

is a sum of two terms. Define some scalar σ to measure distance from the singularity. (In Schwarzschild spacetime, an obvious choice is the area radius R .) For any given α and σ , β^i then can be chosen to set $\dot{\sigma} = 0$, except where $\sigma_{,i} = 0$. (We use a dot to denote $\partial/\partial t$.) In other words, the lapse in a Killing coordinate system vanishes only where the time slices are tangential to the Killing vector field. Every regular time slice in a collapse spacetime, and every wormhole slice through an eternal black hole has such an obstruction point, namely a local minimum of σ (Fig. 1). However, a slice that becomes asymptotically cylindrical (with $R \rightarrow R_0$) and ends at i_L^+ avoids this obstruction (Fig.2).

C. Excision

An alternative to singularity-avoiding slicings is singularity excision. This means truncating the time slices along a future spacelike surface which is also (at least asymptotically) Killing. In Schwarzschild spacetime, this would be a surface of constant $R < 2M$. One still wants the slice to be Lie-dragged along the Killing field, but one gains more freedom because Killing slices are now acceptable which would intersect the singularity, such as Kerr-Schild slices of Schwarzschild. A Killing slicing with Killing excision boundary is illustrated in Fig. 3.

As long as the excision surface is spacelike, all characteristics corresponding to gravitational waves, which propagate on light cones, will be leaving the domain of computation. Depending on the formulation of the Einstein equations and the gauge choice, other characteristics corresponding to constraint modes and gauge modes may be spacelike, and either this will restrict the excision surface further or explicit boundary conditions need to be imposed on the gauge if the evolution equations are to be well-posed. If the system is not hyperbolic, for example because the gauge conditions are parabolic or elliptic, boundary conditions will be required on any excision boundary.

In [10] and [11], evolutions were carried out from puncture data using BMT 1+log slicing with and without K_0 , and directly comparing evolutions using either excision or fixed punctures. No explicit boundary condition was imposed at the excision boundary. Excised and non-excised evolutions are claimed to converge to each other to second order everywhere outside the excised region. This is surprising given that the excision problem was ill-posed.

III. KILLING COORDINATES

A. General case

By definition, coordinates in which the 4-metric is time-independent are those in which $(\partial/\partial t)^a = C\xi^a$, where ξ^a is a Killing vector that is timelike at infinity and $C \neq 0$ is a constant. Contracting with n_a , we find

that the *Killing lapse* is given by

$$\alpha = C\phi, \quad (2)$$

where $\phi \equiv -n_a \xi^a$, and contracting with the projector $\perp_a^b \equiv g_a^b + n_a n^b$ we find that the *Killing shift* is

$$\beta^i = \frac{\alpha}{\phi} (\perp \xi)^i. \quad (3)$$

B. Schwarzschild spacetime in spherical symmetry

We now restrict to spherically symmetric Killing coordinate systems on the Kruskal extension of Schwarzschild spacetime. In the following, X^μ are preferred coordinates on a given spacetime such as Schwarzschild, while (t, x^i) are the coordinates used for the numerical evolution, in our case with the spherical line element

$$ds^2 = -\alpha^2 dt^2 + \gamma(dr + \beta dt)^2 + R^2 d\Omega^2, \quad (4)$$

We use the shorthands $d\Omega^2 \equiv d\theta^2 + \sin^2\theta d\varphi^2$, $R^2 \equiv \gamma_{\theta\theta}$, $\gamma \equiv \gamma_{rr}$ and $\beta \equiv \beta^r$. We use \dot{f} and f' for the partial derivatives with respect to t and r .

We use preferred coordinates (T, R) on Schwarzschild with the property that R is the area radius and the Killing vector is $\partial/\partial T$, normalised to unity at infinity, for example Schwarzschild or Kerr-Schild coordinates. In all such coordinates $g_{TT} = 1 - 2M/R$ and $g_{TT}g_{RR} - g_{TR}^2 = -1$. The generic Killing coordinate system (t, r) with $C = 1$ is then given by the ansatz

$$T = t + F(r), \quad R = R(r). \quad (5)$$

If we are interested only in the slicing, we can fix the spatial coordinate r for convenience. A better choice than using R itself as a coordinate is to make r proper distance along the slice, so that $\gamma = 1$. (We shall also use the symbol l for proper radial distance.) The Killing lapse and shift are

$$\alpha = R', \quad (6)$$

$$\beta = \sqrt{\alpha^2 - 1 + \frac{2M}{R}}. \quad (7)$$

The trace of the extrinsic curvature of the Killing slices is

$$K = 2\frac{\beta}{R} + \frac{\beta'}{R'}, \quad (8)$$

where β is given by (7).

IV. EVOLVED SLICING CONDITIONS

We focus on the family of slicing conditions suggested by Bona and Massó [12] (from now BM)

$$\alpha n^a \nabla_a \alpha \equiv \dot{\alpha} - \beta^i \alpha_{,i} = -\mu_L \alpha^2 K, \quad (9)$$

where K is the trace of the extrinsic curvature of the slice and n^a its unit normal vector. Typically, $\mu_L > 0$ is understood to be a given function $\mu_L(\alpha)$ of the lapse. As n^a is a true vector and α and K are scalars under a change of coordinates x^i on the slice, this slicing condition is independent of the coordinates on the slice and therefore independent of the shift.

Confusingly, the very different slicing condition

$$\dot{\alpha} = -\mu_L \alpha^2 (K - K_0), \quad (10)$$

where $K_0(x^i)$ is the initial value of K [9], is also referred to as Bona-Massó slicing. For clarity, we shall refer to (9) as “BMn” (the derivative is along the slice normals) and to (10) as “BMt” (the derivative is along the time lines).

A third slicing condition [13],

$$\dot{\alpha} = -\mu_L \alpha (\alpha K - D_i \beta^i) \equiv \mu_L \frac{\alpha}{2} (\ln |\det \gamma|), \quad (11)$$

where D_i is the covariant derivative compatible with the 3-metric γ_{ij} , is also related to BM. We shall call it “BMg”, as it can be integrated for any $\mu_L = \mu_L(\alpha)$ to relate α to the 3-metric determinant. For $\mu_L = 2/\alpha$, BMg integrates to $\alpha = f(x) + \ln |\det \gamma_{ij}|$, explaining the name “1+log slicing”. BMn and BMt can be integrated only if the shift is zero.

The geometric specification of BMt and BMg (but not BMn) slicing depends on the shift. Here we shall use the “fn-driver”

$$\dot{\beta}^i - \beta^j \beta_{,j}^i = \mu_S \alpha^2 (f^i - f_0^i), \quad (12)$$

or the “ft-driver”

$$\dot{\beta}^i = \mu_S \alpha^2 (f^i - f_0^i), \quad (13)$$

where f^i is the 3-vector defined by

$$f_i \equiv \gamma^{jk} \gamma_{ij,k} - \frac{\rho}{2} \gamma^{jk} \gamma_{jk,i} \quad (14)$$

in preferred Cartesian coordinates (see Appendix C). With $\rho = 2/3$, these are essentially versions of the (implicit) “Gamma-driver” shift conditions that now dominate numerical relativity.

A simple analysis of BMg as a pure gauge system (similar to Appendix A) on Minkowski spacetime shows that it is well-posed with a fixed shift (see also [14]), but is ill-posed with the fn or ft drivers. We do not consider it further.

In Appendix A we also show that BMt slicing in combination with any shift condition always has both positive and negative gauge coordinate speeds. This means that on any excision surface of constant radial coordinate r there will always be a gauge mode travelling towards increasing r , and so excision is not possible with this slicing condition unless a boundary condition is imposed on the gauge at the excision boundary. A similar result holds for the ft-driver shift condition. We will mainly use either an algebraic Killing shift (area freezing shift) or the fn driver shift.

V. COMPATIBILITY OF KILLING COORDINATES WITH BMN SLICING

A. General

In this section we ask if Killing coordinates exist that are compatible with BMn slicing. Although the BMn slicing condition is geometrically independent of the shift, $\alpha(x^i, t)$ only becomes time-independent if the slicing is a Killing slicing and the shift is a Killing shift. Substituting $\dot{\alpha} = 0$, (2) and (3) into (9), we find the scalar equation

$$\perp \xi^i \phi_{,i} = \mu_L (C\phi) \phi^2 K \quad (15)$$

on the slice. We use the definitions $(\perp \xi)^a = \xi^a - \phi n^a$, $\nabla_{(a} \xi_{b)} = 0$ and $K_{ab} = -\perp \nabla_a n_b$ to rewrite this equation as a partial differential equation for embedding a slice with unit normal vector n^a :

$$Q^{ab} \nabla_a n_b - \frac{1}{2} n^a \nabla_a \psi = 0, \quad (16)$$

where $\psi \equiv -\xi_a \xi^a$ is related to the gravitational potential in a stationary spacetime and

$$Q^{ab} \equiv -\perp \xi^a \perp \xi^b + \mu_L (C\phi) \phi^2 \perp^{ab} \quad (17)$$

is a symmetric tensor intrinsic to the slice.

Given that the unit normal vector of a slice $t = \text{const.}$ is given by

$$n_a = -\alpha \nabla_a t, \quad \alpha = (-\nabla_b t \nabla^b t)^{-1/2}, \quad (18)$$

the principal part of (16) is $Q^{ab} \nabla_a \nabla_b t$. As \perp^{ab} is positive definite and $\mu_L > 0$, two eigenvalues of Q^{ab} are always positive. The third eigenvalue is associated with the eigenvector $\perp \xi^a$ and is given by

$$D = (\mu_L - 1) \phi^2 + \psi. \quad (19)$$

Therefore (16) is elliptic for $D > 0$ and (2+1) hyperbolic for $D < 0$.

Alcubierre [15] has shown that the BMn slicing condition can also be written as the 3+1 wave equation

$$P^{ab} \nabla_a \nabla_b t = 0, \quad P^{ab} \equiv -n^a n^b + \mu_L(\alpha) \perp^{ab} \quad (20)$$

where \perp^{ab} , α and n^a are as given above. We have perturbed this equation around a Killing slicing t , but have not been able to identify any lower-order (friction-like) terms that would always push δt locally towards $\xi^a \nabla_a \delta t = 0$ or $\delta t = 0$. We conclude that if BMn slicing is really symmetry seeking in some circumstances, as our numerical evidence below suggests, this is not because of local friction terms, but rather through the mechanism by which a solution of the wave equation on a finite domain with a dissipative boundary condition settles to a time-independent solution of the Laplace equation.

The characteristics of the wave equation (20) are null surfaces of the ‘‘gauge metric’’ $(P^{-1})_{ab} = -n_a n_b + \mu_L^{-1} \perp_{ab}$, which is the matrix inverse of P^{ab} . A slice

evolving under (20) can be excised on a boundary ruled by trajectories of the Killing vector only if the Killing vector is ‘‘spacelike’’ with respect to the gauge metric, that is $(P^{-1})_{ab} \xi^a \xi^b > 0$. We find that this is once again equivalent to $D < 0$.

B. Schwarzschild spacetime in spherical symmetry

This subsection reviews and generalises [4]. The BMn Killing slicing condition in spherical symmetry is

$$\beta \alpha' = \mu_L(\alpha) \alpha^2 K \quad (21)$$

Using (6) and (8) to eliminate α and K gives

$$-\frac{R''}{R' \mu_L(R')} + \frac{\beta'}{\beta} + 2\frac{R'}{R} = 0, \quad (22)$$

which has an obvious first integral that can be expressed, using (6) and (7), as

$$-2 \int^{R'} \frac{d\alpha}{\alpha \mu_L(\alpha)} + \ln \left[\left(R'^2 - 1 + \frac{2M}{R} \right) R^4 \right] = c. \quad (23)$$

Alternatively, using (7) to eliminate β from (22) gives

$$R'' = -\frac{\mu_L N}{R D}, \quad (24)$$

where

$$N \equiv R'^2 \left(2R'^2 - 2 + \frac{3M}{R} \right), \quad (25)$$

$$D \equiv [\mu_L(R') - 1] R'^2 + 1 - \frac{2M}{R}. \quad (26)$$

[Here D has the same meaning as in (19).] For given $\mu_L(\alpha)$ this is a second order ODE for $R(r)$. For the solution to be regular for all $R > 0$, N and D have to vanish at the same r , which becomes a regular singular point. This fixes R and R' at this r , and hence the constant c in (23). (23) can then be solved as a first-order ODE for $R(r)$. This means that for any $\mu_L(\alpha)$, there are at most a finite number of twice differentiable spherically symmetric Killing slicings of Schwarzschild, one for each possible regular singular point. The 3-dimensional PDE (16) of which (24) is the reduction to spherical symmetry is elliptic for $R > R_c$ and hyperbolic for $R < R_c$. In the absence of spherical symmetry, requiring regularity at the 2-dimensional boundary between elliptic and hyperbolic regions would also make the slice more rigid, as it does in spherical symmetry. The first integral (23), however, has no counterpart in the absence of spherical symmetry.

1+log slicing The case of 1+log slicing, $\mu_L = 2/\alpha$ has been presented in [4], based on earlier work in [16]. There are two possibilities for regular singular points. One is $R = 2M$ with $R' = 0$. This gives a Killing slicing where each slice goes through the bifurcation point of

the horizon, the lapse is positive in R and negative in L, and the slices never reach P or F. It is not of interest for numerical evolutions.

The other regular singular point is $R' = R'_c \equiv -3 + \sqrt{10}$, $R = R_c \equiv M/(4R'_c) \simeq 1.54057M$. In this solution $R \rightarrow \infty$ as $r \rightarrow \infty$ and $R \rightarrow R_0$ from above as $r \rightarrow -\infty$. R_0 can be found from (23) with $R' = 0$, is given in implicit form in [4], and is approximately $R_0 \simeq 1.31241M$. Inside the black hole the slices become asymptotically tangent to the Killing field and terminate at i_L^+ . The intrinsic geometry of each slice becomes a cylinder of radius R_0 as $r \rightarrow -\infty$ (Fig. 2).

Harmonic slicing Harmonic slicing is the special case of BMn slicing with $\mu_L = 1$. The regular singular points are then $R = 2M$ with either $R' = 0$ or $R' = \pm 1/2$. The former can be discarded, and the sign in the latter is trivial, so that the Killing slices are characterised by $\alpha = R' = 1/2$ at $R = 2M$. These slices stretch from i_R^0 to the future singularity $R = 0$, and so must be used with excision. The gauge characteristics are the light cones [17], so the gauge only requires the excision boundary to be spacelike.

General $\mu_L(\alpha)$ Killing slices cannot have an extremum of R if they are to be stationary points of some slicing condition. From (23) we see that if the Killing slices are to approach i_L^+ , that is $\lim_{r \rightarrow \infty} R = R_0 > 0$, the integral

$$\int_0^{\alpha} \frac{d\alpha}{\alpha \mu_L(\alpha)} \quad (27)$$

must be finite, for example with $\mu_L = 2/\alpha$. We conjecture that, conversely, if this integral diverges, as with $\mu_L = 1$, the Killing slices must intersect the future singularity.

Excision and uniqueness One might think that excising a BMn Killing slice would make it less rigid, because the regular singular point $R = R_c$ could be excised. This is correct if one excises at $R_c < R < 2M$ and imposes an explicit boundary condition on the slicing, for example by fixing α at the excision boundary. By function counting one would expect the value of α at the boundary to control the value of the constant c of the slice. However, to excise all modes including the lapse gauge modes, the excision boundary must be in the region where $D < 0$, and so $R = R_c$ must be on the slice. The only possible Killing endstate of the slicing is then the unique one derived above.

VI. VACUUM BLACK HOLE EVOLUTIONS

A. Method

To see empirically if generic black hole evolutions are attracted to the Killing states we have characterised above, we have carried out numerical evolutions of the Schwarzschild spacetime in spherical symmetry, using BMn 1+log slicing.

We can take advantage of the fact that this metric is known in closed form to evolve only the coordinates on the known spacetime, see Appendix A. There is no global coordinate system that covers wormhole slices and which is also Killing. Therefore, in pure gauge evolutions of wormhole slices stretching from i_R^0 to i_L^0 , we restrict to slices with a discrete “left-right” isometry through the coordinate sphere $r = 0$, so that we only evolve explicitly on F and R, where KS coordinates can be used, with a boundary condition at $r = 0$ representing the isometry.

Even this does not work for slices which go through the horizon bifurcation 2-sphere (where KS time and similar Killing time coordinates are $-\infty$), and so for such slices we need to evolve the Einstein equations in the NOR formulation, see Appendix B. In all other cases, plots are from pure gauge evolutions, but we have verified that our results are replicated in evolutions of the full Einstein equations in the NOR formulation. The evolutions described here all use the fn shift condition (12) except otherwise stated.

B. With excision boundary

As initial data for the geometry and the coordinates we have considered:

- 1a) KS slice, KS lapse, KS shift, area radius;
- 1b) KS slice, KS lapse, zero shift, area radius;
- 2) A closed form asymptotically cylindrical slice, unit lapse, zero shift, area radius, see Appendix A 2.
- 3) The Hannam slice, lapse, shift, all in area radius, see Appendix A 2.

We first evolved with area locking (that is, Killing) shift (which is determined algebraically so that the initial value of the shift listed above is irrelevant) and excision. We excised at $R = 1.54M$, which is just inside the maximal excision radius $R = R_c \simeq 1.54057M$ for which all modes are outgoing. We find that 1) and 2) approach the Killing state, and 3) remains there. This is demonstrated in Fig. 5, and indicates that the Killing state has a significant basin of attraction.

When combined with the fn shift driver, in 1a) the coordinates r are pushed out of the black hole and further. 1b), and 2) again settle down to the Hannam endstate, and 3) remains there. With 1b), the excision radius initially has to be $R \simeq 1.3M$ or the excision surface at constant r will be pushed out so far before it reaches steady state that there a gauge mode is ingoing.

C. With isometry boundary condition

We begin with NOR evolutions starting from the time-symmetric wormhole slice that goes through the bifurcation 2-sphere $R = 2M$.

We first use spatial coordinates in which i_L^0 is represented by the point $r = 0$ (the “puncture”), see Appendix B. Evolutions with this method reproduce the

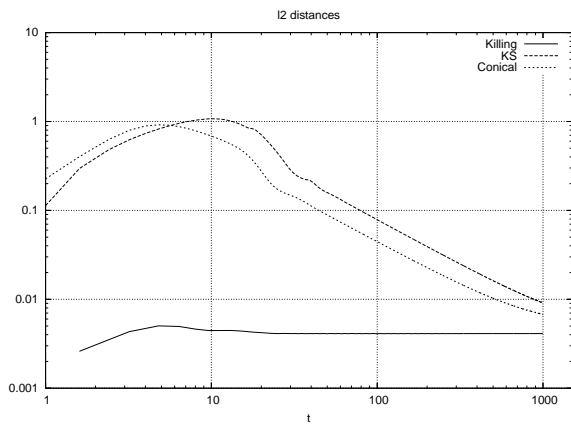


FIG. 5: The L^2 distance of the lapse from the Killing endstate over the range from the excision boundary $R = 1.54$ (just inside the regular singular point) out to $R = 21.54$, with area locking shift. The power law decay indicates $\|\alpha - \alpha_{\text{Killing}}\| \sim t^{-1}$.

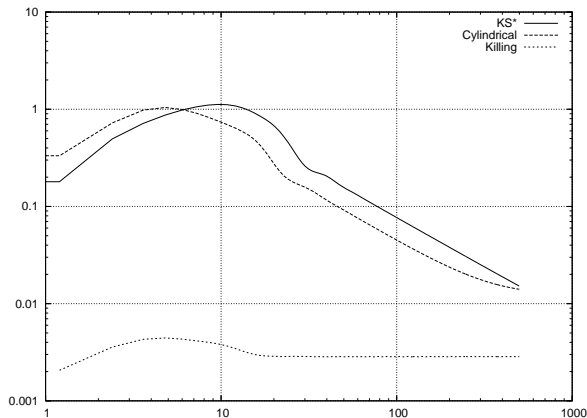


FIG. 6: The L^2 distance of the lapse from the Killing endstate from the excision boundary with approximately the same limits as in Fig. 5, using the fn shift driver (12). The power law decay again indicates $\|\alpha - \alpha_{\text{Killing}}\| \sim t^{-1}$.

behaviour described in [4]: numerical error changes the topology and the evolution settles down to the asymptotically cylindrical Killing state.

If we evolve the same initial data in spatial coordinates that resolve the wormhole (see Appendix B), we see the slices begin to form a cylinder at radius R_0 , but at reasonable resolution constraint violation in the Einstein code makes the result unreliable soon after.

Pure gauge evolutions with wormhole initial data that lie to the future of the bifurcation 2-sphere (so that $R < 2M$ at the throat) and a discrete isometry boundary as described in Appendix A are more stable. At the isometry boundary (where R is minimal) the lapse quickly collapses. In low resolution evolutions, the lapse collapses starting at the minimal R (at the isometry boundary),

and a cylinder of radius R_0 forms with proper length increasing linearly in time (Fig. 7).

D. Gauge shocks

However, higher resolution (for example $\Delta r = M/50$) evolutions show that low resolution only hides the formation of a gauge shock where K forms a large negative peak and α'' forms a positive peak, at $R \simeq 1.5M$. This does not seem to happen exactly at R_c (we varied $\mu_L(\alpha)$ to check this), and so we do not think that it is a kink instability related to the regular singular point of the Hannam slice. Neither is there any indication that the slice has become null. An ODE mechanism by which $K < 0$ makes α grow is also ruled out as not all initial data where $K < 0$ shock.

Rather, we think we see a gauge shock of the type described by Alcubierre [15, 18]. Note that the lapse speeds expressed in terms of proper distance l per coordinate time t , relative to the time lines, are $-\beta \pm \alpha \sqrt{\mu_L} = -\beta \pm \sqrt{2\alpha}$, so that a gauge wave propagating “left”, from high to low α is expected to steepen. By contrast, the wave propagating “right” and forming the cylinder appears to be stable and translating with constant speed dl/dt without changing its shape much. Alcubierre notes that for the particular choice $\mu_L = 1 + k/\alpha^2$ with $k > 0$ the pure gauge system is linearly degenerate, and we have tried this μ_L , but shocks still form, also in agreement with Alcubierre’s numerical observations. Alcubierre argues that gauge shocks are generic for evolved gauge conditions.

Although the NOR evolutions of the time-symmetric slice are less reliable, they suggest that evolutions shock when α has a local minimum not at the isometry boundary (Fig. 9). They also suggest that with $\alpha = 1$ initially the slicing never shocks (Fig. 8). This agrees with the standard numerical literature where the puncture data are approximately the time-symmetric slice through Schwarzschild and the initial lapse is one. It also agrees with the evolution by Brown [19] of these particular initial data. It seems plausible that initial data in a neighbourhood also do not develop shocks, but we have not investigated this.

We note that the shift remains regular during the blow-up, and the same qualitative picture occurs with proper distance radius, zero shift, or fn driver shift.

With BMt slicing and the ft (not fn) shift driver, we see the same gauge shock in both NOR and pure gauge evolutions, but it seems to form earlier and even at low resolution, so that we never see formation of a cylinder before the code crashes.

VII. SCALAR FIELD COLLAPSE EVOLUTIONS

We now consider the behaviour of collapse simulations with BMn 1+log slicing. As a toy model we consider

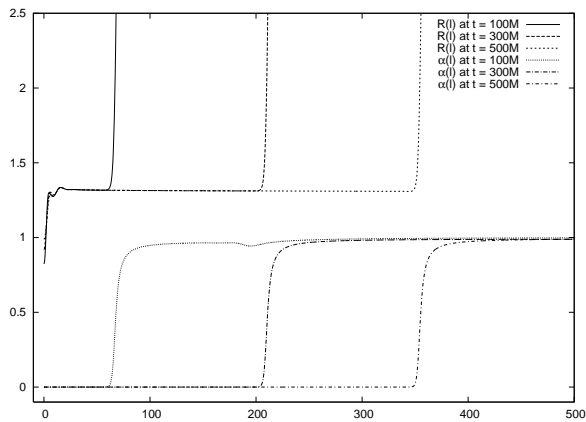


FIG. 7: Snapshots of R and α against proper distance r from an evolution of an isometric slice. The throat of the slice (initially at $R = 1.5M$) is gradually stretched so that it becomes an infinitely long cylinder. The radius of the cylinder agrees with that computed in [4]. Note that low numerical resolution effectively smears out a gauge shock travelling left, so that this is not a correct continuum solution.

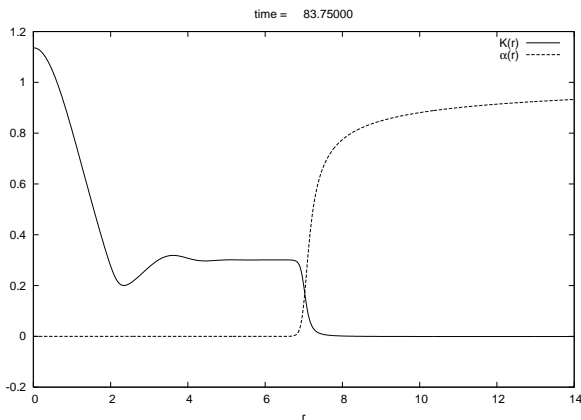


FIG. 8: The $K = 0$ time symmetric slice through the bifurcation surface of Schwarzschild, evolved with BMn 1+log slicing, with $\alpha = 1$ initially. We show a snapshot of K and α against proper distance radius. The edge at $r \simeq 7$ in this snapshot moves to the right, and leaves behind a cylinder of constant R and K with $\alpha \simeq 0$.

a spherical scalar field. We impose spherical symmetry and use proper distance as the radial coordinate. The metric thus takes the form (4) with $\gamma = 1$. Details of the numerical implementation and the initial data are given in Appendix D.

The initial data are chosen as a moment of time symmetry. The scalar field separates into an ingoing pulse and an outgoing pulse. With the chosen parameters, the ingoing pulse collapses to form a black hole, with an apparent horizon first forming at $t = 6.9$. The final mass of the black hole is 1.0. Figs. 10 and 11 show respectively α and K at $t = 14$ and in the range $0 \leq r \leq 3$. Note

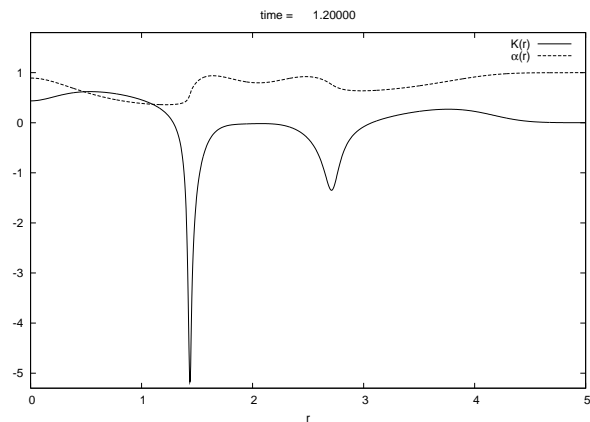


FIG. 9: As in Fig. 8, but with α not constant on the initial slice. The wave on the left travels left and is steepening, about to form a gauge shock, with large negative K . The wave on the right travels right and is also steepening; note $\alpha'' > 0$ there.

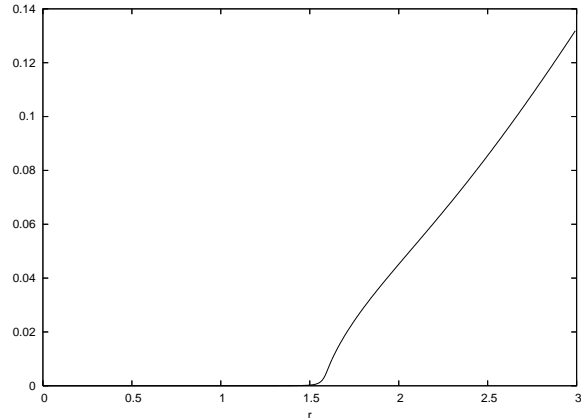


FIG. 10: Plot of the lapse α against proper distance r at $t = 14$ in scalar field collapse without excision.

the sharp features in both these quantities near $r = 1.5$. These features become ever sharper and cause the code to crash not long after the time of these graphs. This pathology is again a gauge shock. Neglecting the shift the principal part of the the evolution equation for K is $\dot{K} = -\alpha''$. Combining this with the BMn equation yields a nonlinear wave equation for the lapse whose principal part is $\ddot{\alpha} = 2\alpha\alpha''$. The modes of this equation travel with speeds $\pm\sqrt{2\alpha}$. Thus if one has an inner region where the lapse has collapsed, then left-moving gauge waves pile up on the boundary of this region, giving rise to a shock wave in α which in turn (through the equation $\dot{K} = -\alpha''$) will induce a shock wave in K . Fig. 12 shows α'' at $t = 14$ and in the range $0 \leq r \leq 3$. Note that this quantity also has a sharp feature near $r = 1.5$.

In this simulation, the pathological behaviour is inside the horizon. This suggests that we might be able to avoid the pathology by using excision. Figs. 14 and 13 respec-

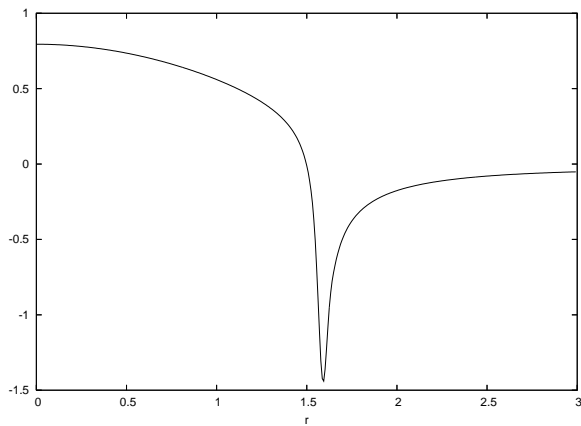


FIG. 11: Plot of K against proper distance r at $t = 14$ without excision.

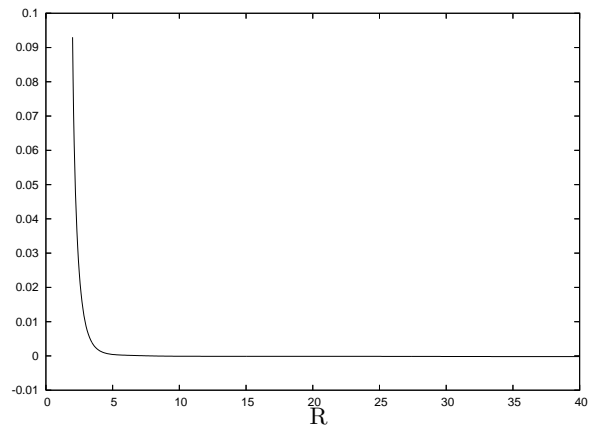


FIG. 13: Plot of K against area radius R at $t = 60.5$ with excision.

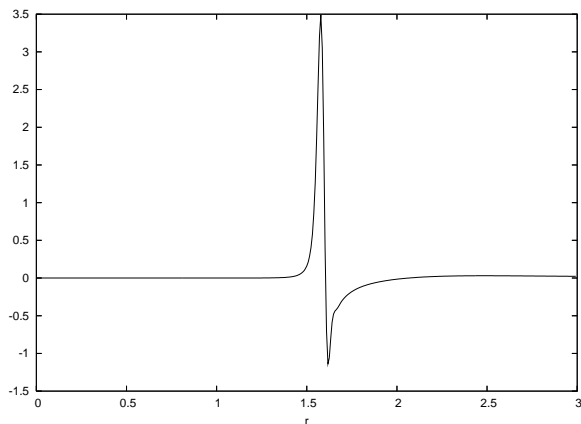


FIG. 12: Plot of α'' against distance r at $t = 14$ without excision.

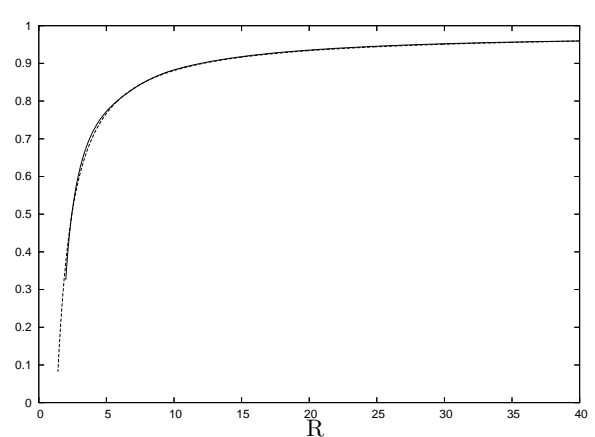


FIG. 14: Plot of α against area radius R at $t = 60.5$ with excision (solid line) and the exact Killing lapse (dashed line).

tively present the values of α and K for a simulation done using excision. Here the simulation is run until $t = 60.5$ and all quantities are plotted as functions of the area radius R rather than proper distance r . It is excision that allows the simulation to be run this long because the excised grid contains no regions of negative K which caused the non-excision simulation to crash. Furthermore, this late in the simulation, these quantities have asymptoted to the static values described in [4]. This is illustrated in Fig. 14 which contains two plots of α as a function of R . The solid line is the α given by the endstate of the excision collapse simulation, while the dotted line represents the Killing lapse given by an integration of the ODEs of [4].

VIII. CONCLUSIONS

Killing endstates We have explained why it is possible in evolutions of black holes that all metric coefficients become time-independent without either slice stretching or collapse of the lapse. We have reviewed the Bona-

Massó slicing conditions, and have derived a mixed elliptic/hyperbolic PDE on the slice that characterises Killing endstates of the BMn family of slicing conditions. Numerically, we have shown that spherical BMn slicings of the Schwarzschild spacetime are attracted to the Killing endstate from nearby initial data. We do not fully understand the mechanism for this. Initial data further away also appear to be attracted to the Killing state, but on closer inspection this is true only at low numerical resolution.

Gauge shocks Increasing the resolution reveals that in the continuum the 1+log BMn slicing *generically* develops gauge shocks of the type described by Alcubierre [18], where the speed of gauge waves associated with the slicing increases with the lapse, so that gauge waves moving from large to small lapse steepen. The only initial data set we have examined that does *not* form a gauge shock with BMn 1+log slicing is the time-symmetric wormhole slice through Schwarzschild spacetime with unit initial lapse, although we suspect that there is at least a neighbourhood of such data. More numerical work is required

to explore this.

It may be that gauge shocks would also occur in binary black hole simulations with 1+log BMn slicing in the continuum, but that they are suppressed by low resolution inside the black holes. By contrast, in collapse simulations the central region is typically adequately resolved, and in fact recent work where the collapsing region is never excised seems to require large dissipation for stability [20].

Excision We find that in both collapse and vacuum simulations the gauge shock can typically be avoided by excising just inside the apparent horizon. There seems to be no clear awareness in the literature that such a boundary still has an incoming gauge mode, and that the resulting continuum problem is ill-posed.

Confirming this, our vacuum (both Einstein and pure gauge) evolutions in spherical symmetry do not converge and often blow up when an incoming mode at the excision boundary is neglected. By contrast, our collapse code, which uses different numerical methods, does not seem to mind. There is also an explicit claim that 3D binary black hole evolutions converge equally well with and without excision [10, 11].

We have also re-derived the previously known [17] fact that if gauge drivers are not of the form $\dot{\alpha} + \beta^i \alpha_{,i} = \dots$ and $\dot{\beta}^i + \beta^j \beta_{,j}^i = \dots$, full excision is not possible at any radius.

Nature of the Killing endstate of BMn slicing If there is to be no incoming gauge mode at an excision boundary, the equation obeyed by the Killing slice has a transition from elliptic to hyperbolic. Requiring regularity there makes the slice more rigid, and in spherical symmetry makes it unique. The same is true if the slice has no excision boundary.

We have clarified that this unique Killing BMn slicing of a Schwarzschild black connects spacelike infinity outside the black hole to future timelike infinity inside the black hole, where it becomes asymptotically cylindrical. As pointed out independently by Brown [19], initial data which connect two asymptotically flat regions through a wormhole cannot evolve to this endstate in the continuum, although numerical under-resolution gives the false impression that the topology jumps. In the continuum evolution, the wormhole stretches into a cylinder whose length grows without bound.

Comments on 3D evolutions In our investigation, we have identified three problems with current gauge choices in 3D numerical evolutions of collapse and black holes with a currently favoured slicing condition, BMn 1+log slicing: 1) wormhole data do not admit a BMn Killing endstate; 2) excision close inside the apparent horizon requires explicit boundary conditions for the gauge; and 3) coordinate shocks form generically. None of these problems have been noted in the binary black hole literature, but we believe that this is only because of limited resolution, and that they will become apparent as a failure of convergence or instabilities at sufficiently high resolution. There are, however, simple ways around these problems:

- Wormhole initial data for eternal black holes ending at i_L^0 should be replaced by initial data that are asymptotically cylindrical and end at i_L^+ .
- Continuum boundary conditions should be imposed explicitly at excision boundaries for any incoming gauge modes.
- The initial lapse should be chosen such that gauge shocks do not form. This will require more empirical studies in 3D. In collapse without excision, changing to a smoothly collapsed lapse profile once an apparent horizon has formed may be helpful.

Final remarks Finally, two technical developments given in the appendix may also be of interest to the 3D community. By characterising pure gauge as the evolution of a coordinate system on a background spacetime given as $X^\mu = X^\mu(x^i, t)$, we have been able to check strong hyperbolicity of the gauge and calculate the gauge speeds without reference to a formulation of the Einstein equations. By re-defining the vector auxiliary variable of the NOR and BSSN formulations (following [21]), we have made them easier to use with non-Cartesian coordinates or multiple coordinate patches.

Acknowledgments

We would like to thank Niall Ó Murchadha for helpful discussions and José M. Martín-García for helpful discussions and comments on the manuscript. DG was supported in part by NSF grant PHY-0456655 through Oakland University.

APPENDIX A: PURE GAUGE EVOLUTIONS

1. General equations

Prescriptions for the lapse and shift can be tested without the specific stability problems associated with any formulation of the Einstein equations by evolving coordinates (t, x^i) on a spacetime given a priori in coordinates X^μ with metric $g_{\mu\nu}$. The ADM evolution equations are replaced by the definition (1) of $\partial/\partial t$ in terms of the lapse and the shift,

$$\dot{X}^\mu = \alpha n^\mu + \beta^i X_{,i}^\mu, \quad (\text{A1})$$

where n^μ are the X^μ components of the unit normal to the t -slices. The 3-metric is given by

$$\gamma_{ij} = g_{\mu\nu} X_{,i}^\mu X_{,j}^\nu, \quad (\text{A2})$$

and $\dot{\gamma}_{ij} = \mathcal{L}_\beta \gamma_{ij} - 2\alpha K_{ij}$ gives

$$K_{ij} = X^\mu_{,ij} n^\nu g_{\mu\nu} + \frac{1}{2} \left(X^\mu_{,i} X^\lambda_{,j} n^\nu + X^\lambda_{,i} X^\nu_{,j} n^\mu - X^\mu_{,i} X^\nu_{,j} n^\lambda \right) g_{\mu\nu,\lambda}, \quad (\text{A3})$$

where the unit normal n^μ is given, up to normalisation, by

$$n^\mu \propto g^{\mu\nu} \epsilon_{\nu\alpha\beta\gamma} X^\alpha_{,1} X^\beta_{,2} X^\gamma_{,3}. \quad (\text{A4})$$

In spherical symmetry n_a is defined by $(\partial/\partial r)^a n_a = 0$, and in preferred coordinates (T, R)

$$n_T = -\frac{R'}{\sqrt{\gamma}}, \quad n_R = \frac{T'}{\sqrt{\gamma}}. \quad (\text{A5})$$

2. Initial data

We use KS coordinates for the background Schwarzschild spacetime. Simple closed form slices which become asymptotically cylindrical at $R = R_0$ may be constructed by making the ansatz $T = t + F(R)$ with

$$F'(R) \simeq -L(R - R_0)^{-1}. \quad (\text{A6})$$

Constructing 1+log Killing data is straightforward in area gauge where $r = R$. We note that proper distance l is $dl = \sqrt{\gamma} dR$ in area gauge $r = R$, while $R' = dR/dl$ in proper distance gauge $r = l$. Therefore, we obtain an algebraic expression for γ in area gauge by replacing R' by $\sqrt{\gamma}$ in (23). A single numerical integral must be performed to compute $F(r)$.

A surface with the required isometry in the F region, with a radial coordinate r in which the isometry is $r \rightarrow -r$, can be given in Schwarzschild coordinates (η, R) as $R(-r) = R(r)$ and $\eta(-r) - \eta_* = -(\eta(r) - \eta_*)$. Here $\eta = \eta_*$ is the reflection surface. Note it is time-like in F. The last condition must be translated into a relation between $T(-r)$ and $T(r)$ using $\eta = T - \phi(R)$ where $\phi(R) \equiv 2M \ln(1 - 2M/R)$. Furthermore, we want the Kerr-Schild time T to be smooth through $R = 2M$, while $\phi(R)$ is not. An ansatz with these properties is

$$T(r) = C(r)r + [1 + D(r)]\phi(R(r)), \quad (\text{A7})$$

where $C(r)$ and $D(r)$ are smooth odd functions and $D(r)$ is 0 at $r = 0$ and -1 on and outside the horizon. To preserve the isometry and the adapted radial coordinate in the evolution the lapse and shift must obey $\alpha(-r) = \alpha(r)$, $\beta(-r) = -\beta(r)$.

3. Characteristic analysis

The spherical gauge evolution system is not quasilinear, because the equations for \dot{R} and \dot{T} are nonlinear in R' and T' . Hence in order to analyse the hyperbolicity of the system one must explicitly linearise, and apply weights to equations and variables [22]. The principal part of the evolution of the coordinates is then

$$\delta\dot{T} \simeq \left(\beta + \frac{\alpha}{\sqrt{\gamma}} (g_{TR} + n^R n^T) \right) \delta T'$$

$$+ \frac{\alpha}{\sqrt{\gamma}} \left(g_{RR} - (n^T)^2 \right) \delta R' + n^T \delta \alpha + T' \delta \beta \quad (\text{A8})$$

$$\begin{aligned} \delta\dot{R} &\simeq \frac{\alpha}{\sqrt{\gamma}} \left(g_{TT} + (n^R)^2 \right) \delta T' \\ &+ \left(\beta + \frac{\alpha}{\sqrt{\gamma}} (g_{TR} + n^R n^T) \right) \delta R' \\ &+ n^R \delta \alpha + T' \delta \beta. \end{aligned} \quad (\text{A9})$$

For BMn slicing with ft shift driver, this is completed by

$$\delta\dot{\alpha} \simeq \frac{\alpha^2 \mu_L}{\gamma} (n_R \delta T'' + n_T \delta R'') + \beta \delta \alpha', \quad (\text{A10})$$

$$\delta\dot{\beta} \simeq -\frac{\alpha^2 (2 - \rho) \mu_S}{\gamma^{3/2}} (n^R \delta T'' + n^T \delta R''). \quad (\text{A11})$$

The system is diagonalisable with real characteristic speeds dr/dt

$$-\beta \pm \frac{\sqrt{\mu_L}}{\sqrt{\gamma}} \alpha, \quad (\text{A12})$$

$$\frac{1}{2} \left(\beta \pm \sqrt{\beta^2 + \frac{4\mu_S \alpha^2 (2 - \rho)}{\gamma}} \right), \quad (\text{A13})$$

and so is strongly hyperbolic.

The principal part of BMn with the fn shift driver (12) is the same except that $\delta\dot{\beta} = \dots + \beta \delta\beta'$. This system is also strongly hyperbolic with characteristic speeds

$$-\beta \pm \frac{\sqrt{\mu_L}}{\sqrt{\gamma}} \alpha, \quad (\text{A14})$$

$$-\beta \pm \frac{\sqrt{\mu_S \sqrt{2 - \rho}}}{\sqrt{\gamma}} \alpha. \quad (\text{A15})$$

For BMn with area locking shift the principal part becomes

$$\delta\dot{T} \simeq \beta \delta T' - \frac{1}{n_T} \delta \alpha, \quad (\text{A16})$$

$$\dot{\alpha} \simeq -\frac{\alpha^2 \mu_L n_T}{\gamma} \delta T'' + \beta \delta \alpha'. \quad (\text{A17})$$

In this case the system is also strongly hyperbolic and has characteristic speeds (A12).

The BMT slicing condition (10) gives rise to strongly hyperbolic pure gauge systems with speeds

$$\frac{1}{2} \left(\beta \pm \sqrt{\beta^2 + \frac{4\mu_L \alpha^2}{\gamma}} \right), \quad (\text{A18})$$

with either area locking shift, ft shift driver [adds speeds (A13)] or fn shift driver [adds speeds (A15)].

Constructing boundary conditions for a system which is not quasilinear is a difficult task which will not be discussed here. Numerically, we have simply frozen all fields at the outer boundary, but we have moved the outer boundary so far out that in the continuum it does not affect the results shown here.

APPENDIX B: WORMHOLE INITIAL DATA FOR THE EINSTEIN EQUATIONS

To create a numerical evolution in spherical symmetry that is similar to the BSSN moving puncture evolutions in 3D, we use the well-known isotropic radial coordinate

$$R(r) = \left(1 + \frac{M}{2r}\right)^2 r, \quad (\text{B1})$$

with range $0 < r < \infty$. We use the correct reduction to spherical symmetry of the NOR system described in Appendix C, stagger the grid around $r = 0$, and impose as boundary conditions at $r = 0$ that γ_{rr} , R and α are even in r , and f^r and β^r are odd. These conditions hold for the puncture initial data, and it is easy to see that they are compatible with the time evolution. If $r = 0$ is a regular centre of spherical symmetry, then $(-r, \theta, \varphi)$ represents the same point as $(r, \pi - \theta, \varphi + \pi)$, and these conditions follow from spherical symmetry and regularity. If $r = 0$ represents i_L^0 then $r < 0$ is simply not part of the spacetime, the even/odd conditions do not follow from spherical symmetry, and their meaning is unclear. However, for finite differencing purposes they are equivalent to finite differencing across the puncture $x = y = z = 0$ in 3D *as if* it was a regular point, which is what is done in 3D puncture evolutions.

In order to resolve both sides of the wormhole, we use the symmetric radial coordinate

$$R(r) = \sqrt{r^2 + 4M^2}, \quad (\text{B2})$$

with range $-\infty < r < \infty$, and impose isometry boundary conditions at $r = 0$.

APPENDIX C: REDUCTION OF THE NOR FORMULATIONS TO SPHERICAL SYMMETRY

To our knowledge, little numerical work using the BSSN or NOR formulations in spherical symmetry has been published, and therefore we would like to point out a technical detail in the reduction to spherical symmetry. f_i can be defined as a true 3-vector by introducing a flat auxiliary connection [21], so that

$$f_a = \gamma^{bc} \hat{\nabla}_c \gamma_{ab} - \frac{\rho}{2} \gamma^{bc} \hat{\nabla}_a \gamma_{bc}. \quad (\text{C1})$$

Here $\hat{\nabla}$ is defined so that its connection coefficients vanish in preferred Cartesian coordinates x^i . In an evolution with a single Cartesian coordinate patch these are the only coordinates, and $\hat{\nabla}_a$ reduces to the partial derivative, but if multiple Cartesian patches are used, one of them is preferred.

In spherical symmetry, $\hat{\nabla}_a$ is defined as the covariant derivative compatible with the flat metric $ds^2 = dr^2 + r^2 d\Omega^2$. The result is

$$f_r = \frac{\gamma'_{rr}}{\gamma_{rr}} + \frac{2}{r} \left(\frac{\gamma_{rr}}{\gamma_T} - 1 \right) - \frac{\rho}{2} \left(\frac{\gamma'_{rr}}{\gamma_{rr}} + 2 \frac{\gamma'_T}{\gamma_T} \right) \quad (\text{C2})$$

where $\gamma_T \equiv R^2/r^2$, we have written γ_{rr} explicitly instead of just γ as elsewhere in this paper, and $f_\theta = f_\varphi = 0$ because of spherical symmetry. Local regularity at the origin $r = 0$ requires $\gamma_{rr} - \gamma_T = O(r^2)$ and $f_r = O(r)$, and so f_a is a regular vector field. [Naively calculating f_r using partial derivatives in (r, θ, φ) gives a different, singular result.]

APPENDIX D: SPHERICAL EINSTEIN-SCALAR CODE

We choose the collapsing matter to be a massless, minimally coupled scalar field ψ so the equations of motion become

$$R_{ab} = \nabla_a \psi \nabla_b \psi, \quad (\text{D1})$$

$$\nabla^a \nabla_a \psi = 0. \quad (\text{D2})$$

We will find it helpful to introduce the quantities A , P , Π , s and w by

$$A = K_{rr} - \frac{1}{3}K, \quad (\text{D3})$$

$$P = \psi', \quad (\text{D4})$$

$$\Pi = n^a \nabla_a \psi, \quad (\text{D5})$$

$$s = \alpha', \quad (\text{D6})$$

$$w = R', \quad (\text{D7})$$

and also to define the quantities $\tilde{\alpha}$ and \tilde{s} by

$$\tilde{\alpha} = \ln \alpha, \quad (\text{D8})$$

$$\tilde{s} = s/\alpha. \quad (\text{D9})$$

The spatial metric evolves by

$$\partial_t \gamma_{ij} = -2\alpha K_{ij} + \mathcal{L}_\beta \gamma_{ij}. \quad (\text{D10})$$

Then noting that $\gamma_{rr} = 1$ we find that the two components of (D10) become

$$0 = -\alpha \left(A + \frac{1}{3}K \right) + \beta', \quad (\text{D11})$$

$$\dot{R} = \beta w + \alpha R \left(\frac{1}{2}A - \frac{1}{3}K \right). \quad (\text{D12})$$

The first of these equations can immediately be integrated to yield

$$\beta = \int \alpha \left(A + \frac{1}{3}K \right) dr. \quad (\text{D13})$$

Differentiating the definition of P with respect to time we obtain

$$\dot{P} = \beta P' + s\Pi + \alpha \left[\Pi' + P \left(\frac{1}{3}K + A \right) \right], \quad (\text{D14})$$

while the wave equation for ψ yields

$$\dot{\Pi} = \beta \Pi' + sP + \alpha \left(K\Pi + P' + \frac{2wP}{R} \right). \quad (\text{D15})$$

The momentum and Hamiltonian constraints yield respectively

$$A' = \frac{-3wA}{R} - \Pi P + \frac{2}{3}K', \quad (\text{D16})$$

$$w' = \frac{1-w^2}{2R} - \frac{R}{4} \left(\Pi^2 + P^2 + \frac{3}{2}A^2 - \frac{2}{3}K^2 \right). \quad (\text{D17})$$

The momentum constraint enables us to differentiate (D12) with respect to r yielding

$$\dot{w} = \beta w' + sR \left(\frac{1}{2}A - \frac{1}{3}K \right) - \frac{1}{2}\alpha R P \Pi. \quad (\text{D18})$$

The BMn slicing condition is

$$\dot{\tilde{\alpha}} = \beta \tilde{s} - 2K, \quad (\text{D19})$$

which when differentiated with respect to r yields

$$\dot{\tilde{s}} = \beta \tilde{s}' + \alpha \tilde{s} \left(A + \frac{1}{3}K \right) - 2K'. \quad (\text{D20})$$

The extrinsic curvature evolves by

$$\begin{aligned} \mathcal{L}_t K^a_b &= \mathcal{L}_\beta K^a_b - D^a D_b \alpha \\ &+ \alpha \left({}^{(3)}R^a_b + K K^a_b - D^a \psi D_b \psi \right), \end{aligned} \quad (\text{D21})$$

where D_a and ${}^{(3)}R^a_b$ are respectively the derivative operator and Ricci tensor associated with the spatial metric γ_{ab} . Eq. (D21) yields the evolution equations

$$\dot{K} = \beta K' - s' - \frac{2ws}{R} + \alpha \left(\frac{1}{3}K^2 + \frac{3}{2}A^2 + \Pi^2 \right) \quad (\text{D22})$$

$$\begin{aligned} \dot{A} &= \beta A' + \frac{2}{3} \left(\frac{ws}{R} - s' \right) \\ &+ \alpha \left(\frac{1}{6}\Pi^2 - \frac{1}{2}P^2 + \frac{1}{4}A^2 - \frac{1}{9}K^2 + KA + \frac{w^2 - 1}{R^2} \right) \end{aligned} \quad (\text{D23})$$

We evolve this system in one of two different ways depending on whether the numerical inner boundary is a regular centre or an excision boundary.

If the inner boundary is a regular centre then the variables to be evolved are $(R, P, \Pi, w, \tilde{\alpha}, \tilde{s}, K)$ which are evolved using Eqs. (D12, D14, D15, D18, D19, D20, D22) respectively. In the evolution equations, the quantities α , s and s' are regarded as derived from the evolved variables

$\tilde{\alpha}$ and \tilde{s} . The shift β is determined from (D13) and the condition that β vanish at the centre. Similarly A is computed by integrating (D16) outward from the centre and using the fact that A vanishes at the centre. Boundary conditions at the centre simply follow from smoothness of the metric which requires that R, P and \tilde{s} vanish there, that the spatial derivatives of $\Pi, \tilde{\alpha}$ and K vanish, and that $w = 1$.

If the numerical inner boundary is an excision boundary, then the variable A is not computed by the momentum constraint but is instead evolved using (D23). The integration constant for (D13) is determined by having the time derivative of the area radius R vanish at the apparent horizon. At the excision boundary, all modes are outgoing, except for a single incoming gauge mode $s - \sqrt{2\alpha}K$. As a boundary condition, its value is prescribed as the value it had at the previous time step. All other modes are evolved at the excision boundary point; however spatial derivatives at that point are computed using one sided differences rather than the centred differences used at the other points [23].

For initial data we choose a moment of time symmetry so that K and Π vanish. The initial value of P is given by

$$P = ar^3 \exp(-r^2/\sigma^2) \quad (\text{D24})$$

where a and σ are constants, and the initial value of R is solved for by using the Hamiltonian constraint. The lapse α is given an initial value of 1. The grid points are equally spaced in r . Spatial derivatives are evaluated using standard second order centred differences and time evolution is done by the iterative Crank-Nicholson method. A marginally outer trapped surface occurs where the derivative of R along the outgoing null direction vanishes. In terms of the variables used here, that corresponds to the vanishing of $w + R(\frac{1}{2}A - \frac{1}{3}K)$. If the apparent horizon (the outermost marginally outer trapped surface) occurs at gridpoint i (and if we choose to excise), then we place the excision boundary at gridpoint $9i/10$. The constants determining the initial value of P were chosen to be $a = 0.05$ and $\sigma^2 = 8$. The number of spatial gridpoints was chosen to be 6401 and the initial range of r was chosen to be $0 \leq r \leq 200$.

[1] F. Pretorius, Phys. Rev. Lett. **95**, 121101 (2005).
[2] M. Campanelli *et al.*, Phys. Rev. Lett. **96** 111101 (2006).
[3] J. G. Baker *et al.*, Phys. Rev. Lett. **96**, 111102 (2006).
[4] M. Hannam *et al.*, Geometry and regularity of moving punctures, eprint gr-qc/060699.
[5] D. Garfinkle and C. Gundlach, Class. Quant. Grav. **16**, 4111 (2002).
[6] S. Brandt and B. Brüggmann, Phys. Rev. Lett. **78**, 3606 (1997).
[7] J. R. Oppenheimer and H. Snyder, Phys. Rev. **56**, 455 (1939).

[8] E. Seidel and W.-M. Suen, Phys. Rev. Lett. (1992).
[9] M. Alcubierre *et al.*, Phys. Rev. D **67**, 084023 (2003).
[10] M. Alcubierre *et al.*, Testing excision techniques for dynamical black hole evolutions, eprint gr-qc/0411137.
[11] M. Alcubierre *et al.*, Phys. Rev. D **72**, 044004 (2005).
[12] C. Bona *et al.*, Phys. Rev. Lett. **95**, 600 (1995).
[13] M. Alcubierre and B. Brüggmann, Phys. Rev. D **63**, 104006 (2001).
[14] M. Alcubierre *et al.*, Class. Quant. Grav. **20**, 3951 (2003).
[15] M. Alcubierre, Class. Quant. Grav. **20**, 607 (2003).
[16] F. Estabrook *et al.*, Phys. Rev. D **7**, 2814 (1973).

- [17] C. Gundlach and J. M. Martín-García, Phys. Rev. D **74**, 024016 (2006).
- [18] M. Alcubierre, Phys. Rev. D **55**, 5981 (1997).
- [19] J. D. Brown, Puncture evolutions of Schwarzschild black holes, eprint arXiv:0705.1359.
- [20] L. Baiotti and L. Rezzolla, Phys. Rev. Lett. **97**, 141101 (2006).
- [21] S. Bonazzola *et al.*, Phys. Rev. D **70**, 104007 (2004).
- [22] M. Renardy and R. C. Rogers, 1993, *An introduction to partial differential equations*, (Springer-Verlag New York)
- [23] F. Pretorius, Class. Quantum Grav. **22**, 425 (2005).